

A Study of Polar Stratosphere-Troposphere Exchange Using AIRS CO₂ and O₃

Xun Jiang^{1,2*}, Moustafa T. Chahine¹, Edward T. Olsen¹, Qinbin Li^{1,3}, Luke L. Chen¹,
and Yuk L. Yung⁴

¹ Science Division, Jet Propulsion Laboratory, California Institute of Technology, USA

² Now at Department of Earth and Atmospheric Sciences, University of Houston, USA

³ Department of Atmospheric and Oceanic Sciences, University of California, Los Angeles, USA

⁴ Division of Geological and Planetary Sciences, California Institute of Technology, Pasadena, USA.

* To whom all correspondence should be addressed. E-mail: xun@gps.caltech.edu

Submitted to JAS, Nov. 12, 2008

Abstract

With the Atmospheric Infrared Sounder (AIRS), we obtained the global distributions of CO₂ and O₃ in the middle to upper troposphere. Our retrieved CO₂ agreed well with the aircraft measurements from *Matsueda et al.* (2002) and GLOBALVIEW-CO₂. The AIRS retrieved O₃ was validated by the independent ozonesonde measurements from the World Ozone and Ultraviolet Radiation Data Centre. The AIRS retrieved CO₂ and O₃ were compared with simulations from 2-D and 3-D chemistry-transport models. The retrieved CO₂ and O₃ were used to understand the large-scale coupling between stratosphere and troposphere in the polar region, especially the final major stratospheric sudden warming (SSW). We investigated the AIRS CO₂ and O₃ before and after a major warming, and found that the retrieved CO₂ increases and retrieved O₃ decreases in the upper troposphere after the major warming. Our results reveal how the chemical tracers (CO₂ and O₃) will response to the large-scale dynamics in the polar region. In addition, this result can be used to better constrain the stratosphere-troposphere exchange in the current three-dimensional chemistry-transport models.

1. Introduction

The polar region has profound significance for climate. The current general circulation models (GCMs) do not work well for the large-scale dynamics in the polar region, particular for the simulations of exchange between the stratosphere and troposphere in that region (Meloan *et al.* 2003). Therefore, observations are essential for understanding the large-scale dynamics and climate changes in the polar region. However, the observations at the polar region are limited so that there are many unknowns. The global distributions of chemical components retrieved from the Atmospheric Infrared Sounder (AIRS) offer a unique opportunity to study the large-scale dynamics in the polar region. In this paper, we use the AIRS data to understand the coupling between the stratosphere and troposphere. Specifically, we study the response of CO₂ and O₃ to the major final Stratospheric Sudden Warming (SSW), which represents an example of strong stratosphere-troposphere coupling.

SSW is an important phenomenon in the winter of stratosphere. Labitzke and Naujokat (2000) have classified the stratospheric warmings into four types. It includes major midwinter warming in January-February, minor warming, Canadian warming, and final warming. During a SSW, the temperature increases and circumpolar winds reverse direction. SSW starts from the upper stratosphere. Some SSWs can penetrate into the middle stratosphere and culminate in a major warming (Quiroz, 1975; Quiroz *et al.*, 1975). Other SSWs are restricted to the upper stratosphere, so that their effect to the whole stratosphere is small. The latter are called minor warmings. SSWs also display

interannual variability, which has been studied by Labitzke (1977). Recently, Limpasuvan *et al.* (2004) examined the composite of 39 major and minor warming events using National Center for Climate Prediction (NCEP)/ National Center for Atmospheric Research (NCAR) reanalysis data and found that the driving by planetary waves leads to the weakening of the stratospheric polar vortex and downward propagation of the positive temperature anomalies during the SSW growth phase. On the other hand, the residual vertical velocity decreases in the polar region during the SSW decaying phase. Using both NCEP/NCAR and ECMWF Reanalysis (EAR-40) datasets, Charlton and Polvani (2007a) constructed a comprehensive climatology for the major midwinter warming events. They classified SSWs into events that do and do not split the stratospheric polar vortex. These two types of events are found to be dynamically distinct. The influence of vortex splitting events on middle-stratospheric temperature lasts longer than the vortex displacement events. Manney *et al.* (2005) studied the SSW in the Arctic winter, and found that there are unusually warm winters in the past seven Arctic winters compared with all events since 1990s.

In this paper, we focus on a major final warming event in the northern hemisphere (NH) in April 2003. Final warmings represent the transition from winter to summer. The time and intensity of final warmings vary from year to year (Labitzke and Naujokat, 2000). The major final warming event in April 2003 has a strong and clear coupling between the stratosphere and troposphere. We study the influence of this major final warming on upper tropospheric tracers, CO₂ and O₃, which are retrieved from the AIRS aboard the NASA EOS-Aqua satellite.

2. Data and Models

2.1. Data

We use CO₂ and O₃ data from AIRS Version 5. AIRS is a cross-track scanning grating spectrometer with 2378 channels from 3.7 to 15.4 μm with a 13.5 km field of view at nadir (Aumann *et al.*, 2003). AIRS data include O₃, CO₂, CO, CH₄, H₂O, T, and other relevant forcing factors such as cloud distribution, cloud opacity, and aerosols (Chahine *et al.*, 2006). Since its launch in May 2002, AIRS has demonstrated a stability of $10^{-3} \text{ K yr}^{-1}$ with a spectral accuracy of the center frequency of 2 parts per million (Aumann *et al.*, 2004). The AIRS retrieval algorithm employs information from a companion microwave sounder, the Advanced Microwave Sounding Unit (AMSU), to retrieve in the presence of clouds on a horizontal scale of one AMSU field of view or $45 \times 45 \text{ km}$ at nadir, the equivalent of 3×3 AIRS footprints (Susskind *et al.*, 2003).

We found that the range $690\text{--}725 \text{ cm}^{-1}$ is best for selecting the main channel set to retrieve the CO₂ mixing ratio (Chahine *et al.*, 2005). The mixing ratios of CO₂ and O₃ are retrieved from the radiance data by the Vanish Partial Derivative Method (VPD) (Chahine *et al.*, 2005; Chahine *et al.*, 2008). The retrieved CO₂ by VPD method captures the correct seasonal cycle compared with those from Matsueda (Chahine *et al.*, 2005). We also validated the CO₂ retrieval with Intercontinental Chemical Transport Experiment – North America (INTEX-NA) (Singh *et al.*, 2002). The precision of the AIRS retrieved CO₂ is within 1-2 ppmv ($\sim 0.5\%$) (Chahine *et al.*, 2008). The maximum of AIRS CO₂ weighting function is between 500 hPa to 300 hPa. The maximal sensitivity for AIRS O₃ is around 300 hPa. To relate the distributions of these tracers to the large-scale dynamics,

we use AIRS retrieved tropopause pressure to differentiate data in the troposphere versus the stratosphere. The tropopause location is defined where the lapse rate changes from positive (in the troposphere) to negative (in the stratosphere).

AIRS CO₂ retrieval will be compared with independent aircraft measurements from Matsueda *et al.* (2002), GLOBALVIEW-CO₂ (GLOBALVIEW-CO₂, 2002), and data from Dr. Michada (personal communication) in Section 3. Aircraft CO₂ from Matsueda *et al.* (2002) are measured biweekly since April 1993 to present. The latitudinal coverage is approximately from 35°S to 35°N. The longitudinal coverage is from 135°E to 150°E. The CO₂ at 8-13 km over the western Pacific from Australia to Japan are measured. We also compared model results with GLOBALVIEW-CO₂ aircraft measurements at Carr (40.9°N, 104.8°W), Estevan Point (49.38°N, 126.55°W), and Poker Flat (65.07°N, 147.29°W). The aircraft vertical profiles from GLOBALVIEW-CO₂ and Dr. Michada (personal communication) are convolved with AIRS weighting function from 800 hPa to the top of aircraft measurements for a direct comparison with AIRS CO₂ retrieval. AIRS 300 hPa O₃ retrieval are validated with the independent ozonesonde data from World Ozone and Ultraviolet Radiation Data Centre (WOUDC). The WOUDC ozonesonde data are downloaded from ftp://ftp.tor.ec.gc.ca/Archive-NewFormat/OzoneSonde_1.0_1/. The ozonesonde climatology data from Logan (1999) are downloaded from <ftp://ftp.as.harvard.edu/pub/sonde/>.

2.1. Model

Caltech/JPL 2-D chemistry-and-transport model (CTM), 3-D GEOS-Chem (v7.3.3), and 3-D MOZART-2 are used to simulate CO₂. The 2-D CTM has 18 latitude boxes, equally spaced from pole to pole, and 40 layers, equally spaced in log (p) from the surface to the upper boundary at 0.01 mbar. In the 2-D CTM, the transport fields are calculated from NCEP Reanalysis 2 (NCEP2). Details are described in our previous study (Jiang *et al.*, 2004). The 3-D GEOS-Chem model is driven by the Goddard Earth Observing System (GEOS-4) assimilated meteorological data from the NASA Global Modeling Assimilation Office (GMAO). The 3-D model has horizontal resolution of 2° (latitude) × 2.5° (longitude). There are 30 vertical levels from the surface to about 70 km in the model. The 3-D MOZART-2 model is driven by the meteorological inputs every 6 hours from the NCEP Reanalysis 1 (Kalnay *et al.*, 1996). Advection in the 3-D MOZART-2 model is computed every 20 minutes with a flux-form semi-Lagrangian method (Lin and Rood, 1996). The horizontal resolution is 2.8° (latitude) × 2.8° (longitude) with 28 vertical levels extending up to approximately 40 km altitude (Horowitz *et al.*, 2003).

The GLOBALVIEW-CO₂ mixing ratio data (Tans *et al.*, 1998; GLOBALVIEW-CO₂, 2007) are used in this study as the lower boundary condition for the Caltech/JPL CTM, GEOS-Chem, and MOZART-2. Since the GLOBALVIEW-CO₂ data has a limited spatial coverage, especially over ocean, we use the GLOBALVIEW-CO₂ to rescale model simulated CO₂ mixing ratios at the surface (Jiang *et al.*, 2008) as a way to constrain the model lower boundary conditions. In a separate simulation using GEOS-Chem, we use prescribed CO₂ sources and sinks as the lower boundary condition, as

described in *Suntharalingam et al.* (2004).

Exchange of CO₂ between the terrestrial biosphere and the atmosphere is based on the net primary productivity and respiration fluxes from the Carnegie-Ames-Stanford (CASA) ecosystem model (Randerson *et al.*, 1997). Air-to-sea exchange of CO₂ is from Takahashi *et al.* (1997). Estimates of fossil fuel emissions are from Marland *et al.* (2007). Monthly mean biomass burning emissions of CO₂ are derived on the basis of Duncan *et al.* (2003). Since there is an unbalanced CO₂ budget associated with the prescribed source and sink boundary conditions (Suntharalingam *et al.*, 2003; Suntharalingam *et al.*, 2004), we rescale the initial global distribution of CO₂ mixing ratio at the beginning of each year with the GLOBALVIEW-CO₂. As a result, the problem of the unbalanced CO₂ budget is mitigated (Jiang *et al.*, 2008).

The 2-D Caltech/JPL CTM used to simulate the O₃ is described in Jiang *et al.* (2004). The model includes all the gas phase chemistry in the NASA recommendations for stratospheric modeling (Sander *et al.*, 2006). There is no heterogeneous chemistry. The transports are the same as that for the CO₂ 2-D model simulation. The O₃ simulation from the 3-D GEOS-Chem is a full chemistry simulation with version 7-04-10 driven by the GEOS-4 meteorology fields (Bey *et al.*, 2001). The CO₂ and O₃ simulations from the above three models will be compared with the AIRS retrieved CO₂ and O₃ in Section 3.

3. Results and Discussions

3.1. Comparison of AIRS CO₂ and O₃ with Models and in-situ Measurements

In this section, we will compare the monthly mean AIRS CO₂ and O₃ in April 2003 with models and in-situ measurements. The latitudinal distribution of the zonal mean AIRS CO₂ (black line) in April 2003 is shown in Fig. 1, along with comparisons to independent CO₂ aircraft measurements and simulations from different models. Standard deviation of CO₂ data is plotted as pink error bars. Grey line is the count of clusters within each zonal strip. Red dots are the Matsueda data from 8 to 13 km. Green and blue dots are the weighted aircraft data from GLOBALVIEW CO₂ and from *Michada*. The aircraft vertical profiles are convolved with the AIRS weighting function from 800 hPa to the top of measurements. Purple is the CO₂ simulation from 2D Caltech/JPL CTM. Green and Yellow lines are the CO₂ simulations from GEOS-Chem driven by the GLOBALVIEW-CO₂ and source/sink flux boundary conditions, respectively. Blue line is the CO₂ simulation from MOZART-2 model. All model CO₂ vertical profiles are convolved with the AIRS weighting function. AIRS retrieved CO₂ agrees very well with aircraft data (color dots) in the tropics and mid-latitude. AIRS CO₂ also captures the correct latitudinal and inter-hemispheric gradients in comparison with the aircraft data. Both observations and models show that there is more CO₂ in the NH than in the SH, due to larger surface sources in the NH. All models underestimate the CO₂ in the high latitudes for both hemispheres, possibly indicating that the exchanges between stratosphere and troposphere in these models are too fast in the high latitudes for this month.

AIRS retrieved O₃ (black line) at 300 hPa is plotted against the ozonesonde data (blue dots), and model simulations in Fig. 2. Purple line is O₃ simulation from Caltech/JPL 2D

CTM. Green line is O₃ simulation from 3-D GEOS-Chem model. Red line is ozonesonde climatology from *Logan* (1999). The latitudinal distribution of AIRS retrieved O₃ is consistent with the ozonesonde data (blue dots) and model simulations in most latitudes in April 2003. The GEOS-Chem 300 hPa O₃ is relatively low in the high latitudes in April 2003, which may be due to an underestimate of downward O₃ flux from the stratosphere at those latitudes in the model.

3.2. Influence of Major Warming on Tracers

We choose a major stratospheric warming event to study its influence on tracer temporal variation. Stratospheric warmings have important influence on the exchange between the stratosphere and troposphere. During the stratospheric warming events, polar stratospheric temperature rise and circumpolar flow reverse direction in a few days. After the events, the vortex will gradually fade away with a shrinking spatial coverage. Therefore, a critical point in our discussion is to track the vortex strength during stratospheric warming events. To represent the vortex strength, we calculate the first principal component (PC1) of the daily time series from the NCEP2 geopotential height (GPH). First, we apply principal component analysis (PCA) method (Richman, 1986; Preisendorfer, 1988; Thompson and Wallace, 2000; Jiang *et al.*, 2008) to the deseasonalized and weighted monthly mean GPH from 20°N to 90°N from 2000 to 2007. Seasonal cycles for each time series are removed; cycles are determined by taking averages for each month independently. The details for the PCA decomposition of the scaled, deseasonalized GPH anomaly, Ω_A , can be represented as:

$$\Omega_A(t, \theta, \varphi) = \sum_i p_i(t) e_i(\theta, \varphi), \quad (1)$$

where t is time, θ is longitude, φ is longitude, p_i is i^{th} PC, e_i is the i^{th} EOF, and the summation is over all the eigenfunctions with eigenvalues arranged in descending order. In order to recover the spatial patterns for the original (unscaled) GPH anomaly, we perform a multiple linear regression for each grid point (θ, φ) , using as predictors the PC time series, $p_i(t)$. The resulting linear regression coefficients, $C_i(\theta, \varphi)$, are the spatial patterns of the GPH variability associated with the i^{th} PC time series, $p_i(t)$. Finally, we regress the first four dominant spatial patterns, $C_i(\theta, \varphi)$, on the daily GPH to obtain the daily PC1 timeseries.

We apply the same method for the data at 17 pressure levels from 1000 to 10 hPa. The spatial patterns for the first modes at 500 hPa, 100 hPa, and 30 hPa are shown in Figs. 3a-3c. The first modes at 500 hPa, 100 hPa, and 30 hPa capture 14.7%, 35.2%, and 54.3% of the total variance, respectively. The values for the first modes are negative (positive) in the polar region (low latitudes). The daily PC1 is plotted in Fig. 3d as a function of altitude. Positive value for PC1 represents a strong polar vortex, while negative value for PC1 represents a weak polar vortex. PC1 switches sign around Apr 15, 2003 in the stratosphere. Polar vortex will shrink and be destroyed after Apr 15, 2003, which is the same date when the circum-polar 10 hPa wind reversed direction and the major final warming happened (Chahine *et al.*, 2008). After the SSW event, there will be less downwelling in the polar region. It has important impact on the tracers.

An illustration of how the major final warming influences tracer is shown in Fig. 4. As shown in Fig. 4a, CO₂ concentration in the troposphere is low inside the vortex due to

the mixing of stratospheric CO₂-poor air into the troposphere. Since O₃ concentration is high in the stratosphere, O₃ concentration in the troposphere is high inside polar vortex. The shrinking of vortex area after the major final warming leads to the transport of mid-latitude CO₂-rich air into the polar region. Meanwhile, mid-latitude air with relatively low concentrations of O₃ is transported into the polar region. As a result, the polar CO₂ should increase while O₃ should decrease after the major final warming in the horizontal direction. In the vertical direction, there will be less downwelling after the major final warming event. Since the source for CO₂ is at the surface, there is more CO₂ in the troposphere than that in the stratosphere as illustrated in Fig. 4b. There is more O₃ in the stratosphere than that in the troposphere, since O₃ is created in the tropical stratosphere and transported to the polar stratosphere. Less downwelling will lead to weaker mixing between troposphere and stratosphere. Therefore, a decrease in O₃ and an increase in CO₂ will be expected as a result of the weaker mixing in the vertical direction.

Our global distribution of CO₂ and O₃ from AIRS offer a unique opportunity to investigate the influence of stratospheric warming on tracers in the upper troposphere. We also study the dynamical variable, tropopause pressure, during the same time period. The spatial patterns of AIRS CO₂, O₃, and tropopause pressure in the first and last ten days of April 2003 are plotted in Fig. 5. The black contours in Fig. 5 are the 500 hPa NCEP2 GPH. Figure 5 shows that the mid-latitude CO₂ is transported to the high latitudes after the major final warming event, while the mid-latitude O₃ is transported to the high latitudes after this event. The polar AIRS CO₂ increases and polar AIRS O₃ decreases after the major final warming. The tropopause pressure decreases and

tropopause height increases after the major final warming, which is a result of vortex weakening. Tracers in the troposphere will have less influence from stratosphere after the tropopause height increases. In the GEOS-Chem simulation, there is some enhancement of CO₂ and decrease of O₃ after the major final warming. However, the magnitude is much smaller. Some studies already show that most of GCMs have less stratospheric warming events compared with observation (Charlton and Polvani, 2007b). It might be related to a lack of meridional heat flux in the lower stratosphere. In addition, the vertical motion is a challenge for model to simulate it correctly.

In summary, we have obtained the global distribution of CO₂ on a weekly basis for the first time. The quality of AIRS retrieved CO₂ and O₃ in the upper troposphere is very good even in the high latitudes. After the stratospheric major final warming, the retrieved CO₂ increases and retrieved O₃ decrease in the upper troposphere. This is consistent with the influence of vortex area shrinking and less downwelling in the polar region. It is still a challenge to simulate the influence of stratospheric sudden warming on tracers using the current chemistry-transport model. We hope to use the AIRS CO₂ and O₃ to better constrain the stratosphere-troposphere exchange in the models in the future.

Acknowledgement: This work is performed at JPL under contract with NASA, and is supported by project 102438-04.02.01. We thank T. Pagano and J. Margitan for helpful comments. Qinbin Li is supported in part by NASA Atmospheric Composition Modeling and Analysis program. Yuk Yung is supported in part by NASA grants NNG04GD76G and NNG04GN02G to the California Institute of Technology.

References:

- Aumann, H. H., *et al.*, 2003: AIRS/AMSU/HSB on the Aqua mission: design, science objectives, data products, and processing systems. *IEEE Trans. Geosci. Remote Sens.*, **41**, 253.
- Aumann, H. H., D. Gregorich, S. Gaiser, and M. Chahine, 2004: Application of atmospheric infrared sounder data (AIRS) to climate research. *Proc. SPIE Int. Soc. Opt. Eng.*, **5570**, 202-208.
- Bey, I., *et al.*, 2001: Global modeling of tropospheric chemistry with assimilated meteorology: model description and evaluation. *J. Geophys. Res.*, **106**, 23073-23095.
- Chahine, M., C. Barnet, E. T. Olsen, L. Chen, and E. Maddy, 2005: On the determination of atmospheric minor gases by the method of vanishing partial derivatives with application to CO₂. *Geophys. Res. Lett.*, **32**, doi:10.1029/2005GL024165.
- Chahine, M., *et al.*, 2006: AIRS improving weather forecasting and providing new data on greenhouse gases. *Bulletin of the American Meteorological Society*, **87**, 911-926.
- Chahine, M., *et al.*, 2008: First satellite remote sounding of the global distribution of mid-tropospheric CO₂. Submitted to GRL.
- Charlton, A. J., and L. M. Polvani, 2007a: A new look at stratospheric sudden warmings. Part I: climatology and modeling benchmarks. *Journal of Climate*, **20**, 449-469.
- Charlton, A. J., and L. M. Polvani, 2007b: A new look at stratospheric sudden warmings. Part II: Evaluation of Numerical Model Simulations. *Journal of Climate*, **20**, 470-488.

- Duncan, B. N., *et al.*, 2003: Interannual and seasonal variability of biomass burning emissions constrained by satellite observations. *J. Geophys. Res.*, **108**, doi:10.1029/2002JD002378.
- GLOBALVIEW-CO₂, 2007: *Cooperative Atmospheric Data Integration Project: Carbon Dioxide* [CD-ROM], NOAA ESRL, Boulder, Colorado (Also available on Internet via anonymous FTP to <ftp.cmdl.noaa.gov>, Path: ccg/co2/GLOBALVIEW).
- Horowitz, L. W., *et al.*, 2003: A global simulation of tropospheric ozone and related tracers: description and evaluation of MOZART, version 2. *J. Geophys. Res.*, **108**, doi:10.1029/2002JD002853.
- Jiang, X., C. D. Camp, R. Shia, D. Noone, C. Walker, and Y. L. Yung, 2004: Quasi-biennial oscillation and quasi-biennial oscillation-annual beat in the tropical total column ozone: A two-dimensional model simulation. *J. Geophys. Res.*, **109**, Art. No. JD004377.
- Jiang, X., *et al.*, 2008: Simulation of upper tropospheric CO₂ from chemistry and transport models. *Submitted to Global Biogeochemical Cycles*.
- Kalnay, E., *et al.*, 1996: The NCEP/NCAR 40-year reanalysis project. *Bulletin of the American Meteorological Society*, **77**, 437-471.
- Labitzke, K., 1977: Interannual variability of the winter stratosphere in the Northern Hemisphere. *Mon. Wea. Rev.*, **105**, 762-770.
- Labitzke, K. and B. Naujokat, 2000: The lower arctic stratosphere in winter since 1952. *SPARC Newsletter*, **15**, 11-14.
- Limpasuvan, V., D. W. J. Thompson, and D. L. Hartmann, 2004: The life cycle of the northern hemisphere sudden stratospheric warmings. *J. Climate*, **17**, 2584-2596.

- Lin, S. J., and R. B. Rood, 1996: Multidimensional flux form semi-Lagrangian transport schemes. *Mon. Weather Rev.*, **124**, 2046-2070.
- Logan, J. A., 1999: An analysis of ozonesonde data for the troposphere: Recommendations for testing 3-D models, and development of a gridded climatology for tropospheric ozone. *J. Geophys. Res.*, **104**, 16115-15149.
- Manney, G. L., *et al.*, 2005: The remarkable 2003-2004 winter and other recent warm winters in the Arctic stratosphere since the late 1990s. *Journal of Geophysical Research*, **110**, doi:10.1029/2004JD005367.
- Marland, G., T. A. Boden, and R. J. Andres, 2007: Global, Regional, and National CO₂ Emissions. In *Trends: A Compendium of Data on Global Change. Carbon Dioxide Information Analysis Center*, Oak Ridge National Laboratory, U.S. Department of Energy.
- Matsueda, H., H. Y. Inoue, and M. Ishii, 2002: Aircraft observation of carbon dioxide at 8-13 km altitude over the western Pacific from 1993 to 1999. *Tellus*, **54**, 1-21.
- The data are available at <http://gaw.kishou.go.jp/wdcgg.html>.
- Meloan, J., *et al.*, 2003: Stratosphere-troposphere exchange: A model and method intercomparison. *J. Geophys. Res.*, **108**, doi:10.1029/2002JD002274.
- Preisendorfer, R. W., 1988: *Principal component analysis in meteorology and oceanography*. Elsevier Science, 425 pp.
- Quiroz, R. S., 1975: The stratospheric evolution of sudden warmings in 1969-74 determined from measured infrared radiation fields. *J. Atmos. Sci.*, **32**, 213-224.

- Qurioz, R. S., A. J. Miller, and R. M. Nagatani, 1975: Comparison of observed and simulated properties of sudden stratospheric warmings. *J. Atmos. Sci.*, **32**, 1723-1736.
- Randerson, J. T., *et al.*, 1997: The contribution of terrestrial sources and sinks to trends in the seasonal cycle of atmospheric carbon dioxide. *Global Biogeochem. Cycles*, **11**, 535-560.
- Richman, M. B., 1986: Rotation of principal components. *Journal of Climatology*, **6**, 293-335.
- Sander, S. P., *et al.*, 2006: *Chemical kinetics and photochemical data for use in atmospheric studies 06-2*. Jet Propulsion Laboratory.
- Shim, C., Y. Wang, and Y. Yoshida, 2008: Evaluation of model-simulated source contributions to tropospheric ozone with aircraft observations in the factor-projected space. *Atmos. Chem. Phys.*, **8**, 1751-1761.
- Singh, H., D. Jacob, L. Pfister, and J. Crawford, 2002: INTEX-NA: Intercontinental Chemical Transport Experiment-North America
<http://cloud1.arc.nasa.gov/docs/intex-na/white_paper.pdf>. Data from the 2004 campaign are available at <<http://www-air.larc.nasa.gov/cgi-bin/arcstat/>>.
- Suntharalingam, P., *et al.*, 2003: Estimating the distribution of terrestrial CO₂ sources and sinks from atmospheric measurements: sensitivity to configuration of the observation network. *J. Geophys. Res.*, **108**, doi:10.1029/2002JD002207.
- Suntharalingam, P., *et al.*, 2004: Improved quantification of Chinese carbon fluxes using CO₂/CO correlations in Asian outflow. *J. Geophys. Res.*, **109**, doi:10.1029/2003JD004362.

- Susskind, J., C. Barnett, and J. Blaisdell, 2003: Retrieval of atmospheric and surface parameters from AIRS/AMSU/HSB data in the presence of clouds. *IEEE Trans. Geosci. Remote Sens.*, **41**, 390-409.
- Tans, P.P., *et al.* (Eds.), 1998: Carbon Cycle, in *Climate Monitoring and Diagnostics Laboratory No. 24 Summary Report 1996-1997*, edited by D.J. Hoffmann *et al.*, chap. 2, pp. 30-51. *NOAA Environ. Res. Lab., Boulder Colo.* (Data available from <http://www.cmdl.noaa.gov/>).
- Takahashi, T., *et al.*, 1997: Global air-sea flux of CO₂: An estimate based on measurements of sea-air pCO₂ difference. *Proc. Natl. Acad. Sci. U. S. A.*, **94**, 8292-8299.
- Thompson, D.W.J., and J.M. Wallace, 2000: Annular modes in the extratropical circulation. Part I: Month-to-month variability. *Journal of Climate*, **13**, 1000-1016.

Figure Captions:

Figure 1: Comparison between AIRS Version 5 retrieved CO₂ with aircraft measurements and model simulations in April 2003. Black line: AIRS zonal mean CO₂. Pink error bars: standard deviation of AIRS CO₂. Red dots: Matsueda's aircraft data. Green dots: GLOBALVIEW-CO₂ aircraft data. Blue dots: aircraft CO₂ from Michada. Grey line: count of clusters within each zonal strip. The CO₂ mixing ratios from the GEOS-Chem model (GLOBALVIEW-CO₂ and source/sink boundary conditions) are shown by the green and orange lines, respectively. The CO₂ mixing ratios from the Caltech-JPL 2-D CTM and MOZART-2 are shown by purple and blue lines, respectively.

Figure 2: Comparison between AIRS Version 5 retrieved O₃ with ozonesonde and model simulations in April 2003. Black line: AIRS zonal mean O₃. Pink error bars: standard deviation of O₃. Blue dots: ozonesonde. Grey line: count of clusters within each zonal strip. Red line: ozonesonde climatology from Logan (1999). O₃ mixing ratios simulated by 2-D CTM and 3-D GEOS-Chem are shown as purple and green lines, respectively.

Figure 3: Spatial pattern of the first modes at (a) 500 hPa, (b) 100 hPa, and (c) 30 hPa. Units for the first modes are in meter. (d) Daily PC1 of NCEP2 geopotential height as a function of altitude.

Figure 4: Illustration of the influence of major final warming on CO₂ and O₃ in the upper troposphere. (a) Horizontal direction, (b) Vertical direction.

Figure 5: (a) Stereographic map of AIRS CO₂ during April 1 to April 10 in 2003. (b) Same as (a) for April 21 to April 30 in 2003. (c) Same as (a) for AIRS O₃. (d) Same as (b) for AIRS O₃. (e) Same as (a) for AIRS tropopause pressure. (f) Same as (b) for AIRS tropopause pressure.

Figure 1: Comparison between AIRS Version 5 retrieved CO₂ with aircraft measurements and model simulations in April 2003.

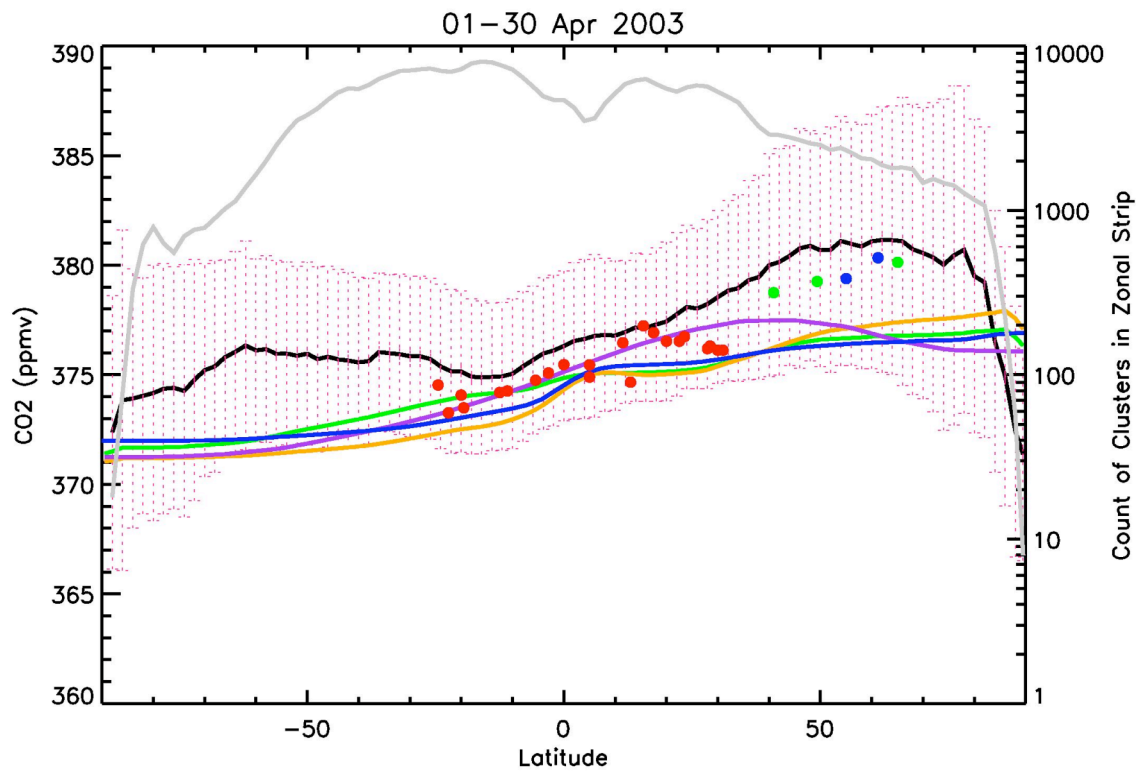


Figure 2: Comparison between AIRS Version 5 retrieved O_3 with ozonesonde and model simulations in April 2003.

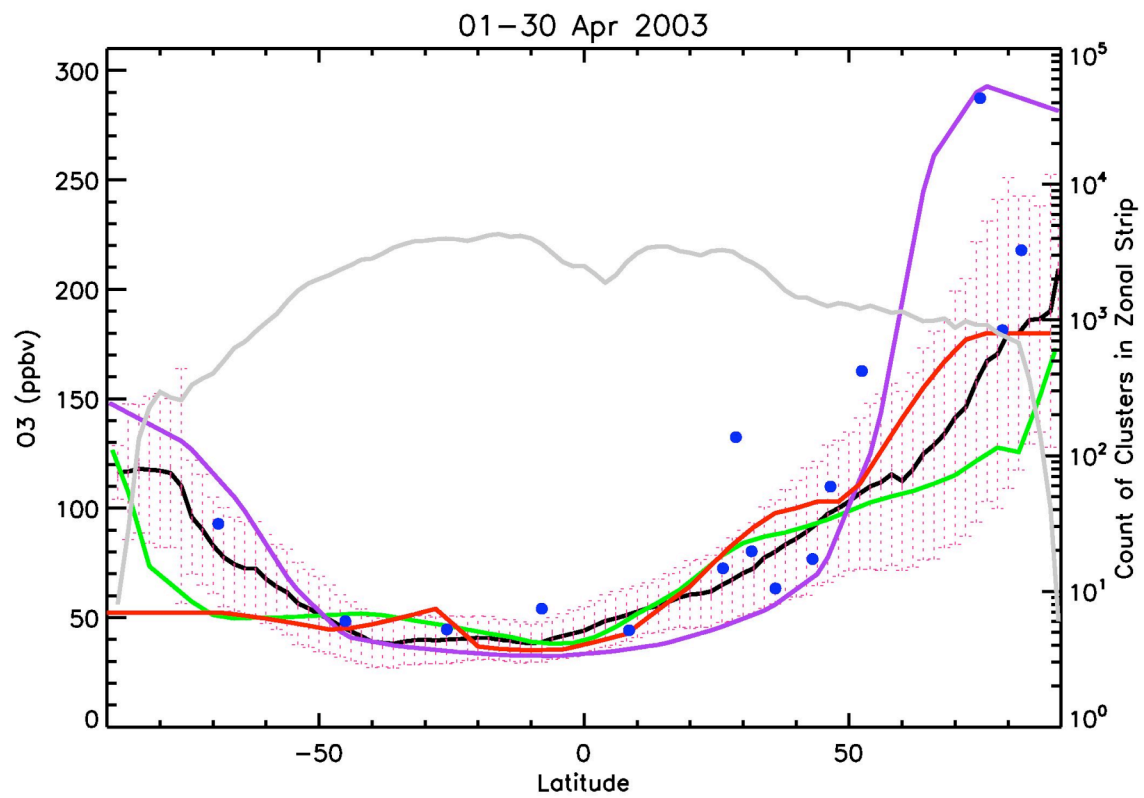


Figure 3: Spatial pattern of the first modes at (a) 500 hPa, (b) 100 hPa, and (c) 30 hPa. Units for the first modes are in meter. (d) Daily PC1 of NCEP2 geopotential height as a function of altitude.

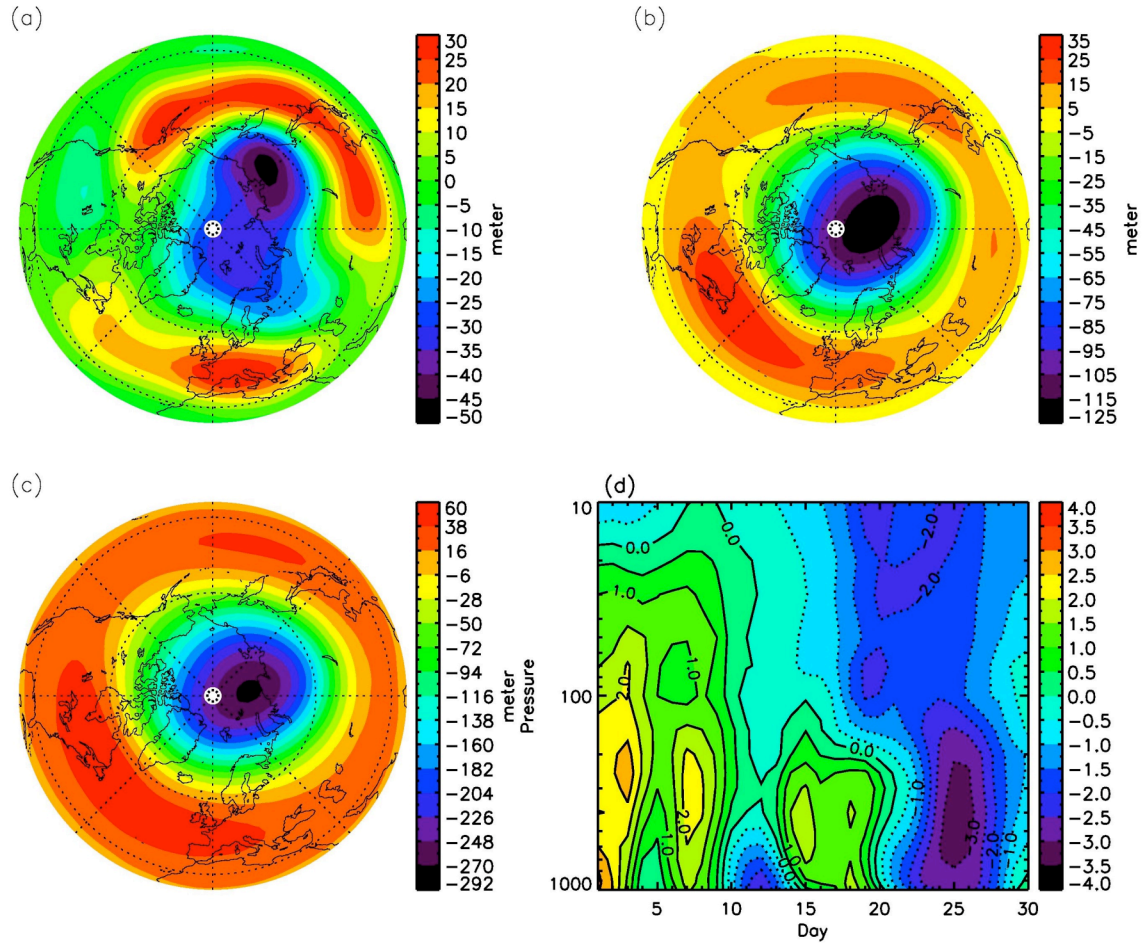


Figure 4: Illustration of the influence of MAJOR FINAL WARMING on CO₂ and O₃ in the upper troposphere. (a) Horizontal direction, (b) Vertical direction.

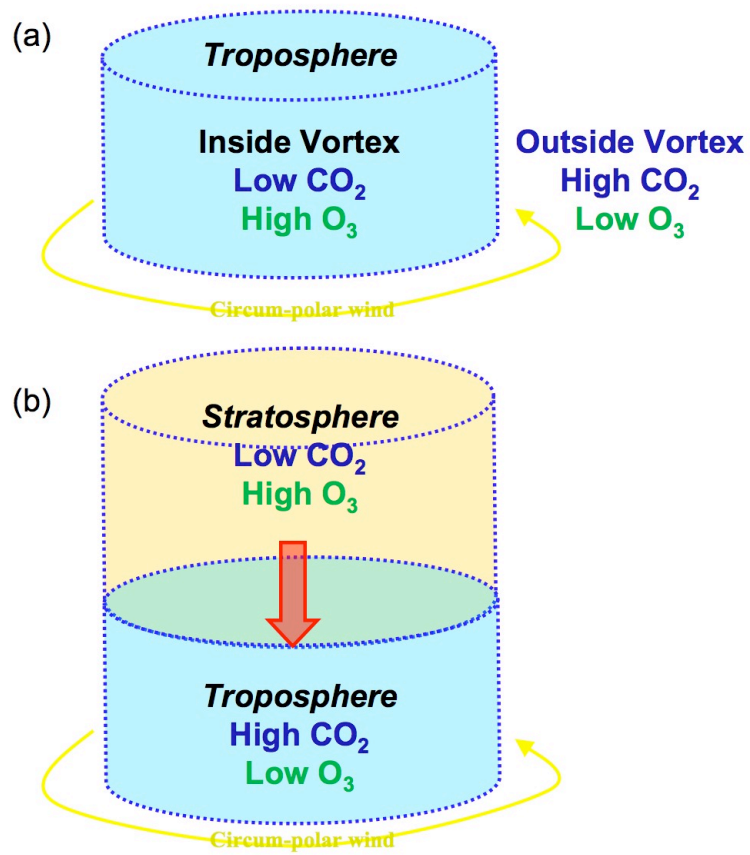


Figure 5: (a) Stereographic map of AIRS CO₂ during April 1 to April 10 in 2003. (b) Same as (a) for April 21 to April 30 in 2003. (c) Same as (a) for AIRS O₃. (d) Same as (b) for AIRS O₃. (e) Same as (a) for AIRS tropopause pressure. (f) Same as (b) for AIRS tropopause pressure.

